PerSort facilitates characterization and elimination of persister subpopulation in mycobacteria

Vivek Srinivas[1], Mario L. Arrieta-Ortiz[1], Eliza J.R. Peterson[1*], Nitin S. Baliga[1-4*]

[1]Institute for Systems Biology, Seattle, WA, USA
[2]Departments of Biology and Microbiology, University of Washington, Seattle, WA, USA
[3]Molecular Engineering Program, University of Washington, Seattle, WA, USA
[4]Lawrence Berkeley National Lab, Berkeley, CA, USA

*Corresponding authors
Eliza J.R. Peterson: eliza.peterson@isbscience.org;
Nitin S. Baliga: nitin.baliga@isbscience.org (lead contact)

Summary

We have developed a novel method, PerSort, to isolate translationally dormant cells that pre-exist in small numbers within *Mycobacterium spp.* cultures growing under naïve conditions (i.e., absence of antibiotic treatment), but dramatically increase in proportion under stress conditions. The translationally dormant cells have high tolerance to isoniazid and rifampicin, and can regenerate the parental population structure in standard media, albeit after a significantly longer lag phase, indicating they are persister cells. Single-cell expression profiling demonstrated that the translationally dormant persister subpopulation is a mixture of *vapC30*, *mazF*, and *relA/spoT* overexpressing cells, indicating there are multiple pathways to become a persister cell. Regardless of the mechanism by which they are generated, the persister cells have reduced oxidative metabolism, which is reversed upon addition of L-cysteine to effect complete clearance by INH and RIF under host-related stress.

Abstract

Mycobacterium tuberculosis (MTB) generates phenotypic diversity to persist and survive the harsh conditions encountered during infection. MTB avoids immune effectors and antibacterial killing by entering into distinct physiological states. The surviving cells, persisters, are a major barrier to the timely and relapse-free treatment of tuberculosis (TB). We present for the first time, PerSort, a method to isolate and characterize persisters in the absence of antibiotic, or other pressure. We demonstrate the value of PerSort to isolate translationally dormant cells that pre-exist in small numbers within *Mycobacterium spp.* cultures growing under optimal conditions, but which dramatically increased in proportion under stress conditions. The translationally dormant subpopulation exhibited multidrug tolerance and regrowth properties consistent with persister cells. Furthermore, PerSort enabled single-cell transcriptional profiling that provided evidence that the translationally dormant persisters were generated through a variety of mechanisms, including *vapC30*, *mazF*, and *relA/spoT* overexpression. Finally, we demonstrate that notwithstanding the varied mechanisms by which the persister cells were generated, they converge on a similar low oxygen metabolic state that was reversed through activation of respiration to rapidly eliminate persisters fostered under host-relevant stress conditions. We conclude that PerSort provides a new tool to study MTB persisters, enabling targeted strategies to improve and shorten the treatment of TB.

Keywords: Mycobacterium, phenotypic heterogeneity, persisters, antibiotic tolerance, nutrient starvation

Introduction

Studies have revealed cell-to-cell variability in organisms from all domains of life –unicellular to multicellular. Through cell-to-cell variability, cell populations are prepared for sudden environmental changes by harbouring subpopulations that are phenotypically pre-adapted. This evolutionary strategy, known as bet-hedging (1), confers fitness advantage to pathogens, such as *Mycobacterium tuberculosis* (MTB), which routinely experience varying environments within the host. In addition to spontaneous bet-hedging, MTB responds to host derived stresses with physiological changes (e.g., shifts in metabolism and respiration, induction of toxin-antitoxin systems, cell wall modifications) that allow it to survive and persist. These physiological changes (either stochastically- or environmentally-induced) result in antibiotic tolerance, in which MTB is genetically susceptible to antibiotics but exists in a physiological state rendering it refractory to drug killing. These persistent states are a major reason why long courses of antibiotic therapy are required to treat human tuberculosis (TB) (2); standard chemotherapy of TB requires 6 months of treatment and 5% are not cured even then (3, 4). There is an urgent need for new

69 strategies that shorten the duration of treatment and target drug tolerant MTB. Addressing this
70 gap requires a better understanding of how MTB generates phenotypic heterogeneity to
71 withstand pressures from the host environment and evade antibiotic therapy.
72 Recent work has studied phenotypic heterogeneity in MTB from single-cell analyses
73 using fluorescent reporter strains. Cell-to-cell variability of MTB was captured *in vitro* and
74 during murine infections using a reporter of 16s rRNA gene expression (5). The microscopy-
75 based platform was able to track heterogeneity in growth rate under standard growth
76 conditions and found heterogeneity was amplified by stress conditions and murine infection.
77 However, the non-growing subpopulation was not isolated and characterized further, most
78 likely due to low fluorescence levels of the reporter. In another study, Jain *et al* developed a
79 dual-reporter mycobacteriophage (ϕ^2DRM) system and used fluorescent activated cell sorting
80 (FACS) to isolate drug tolerant MTB cells from *in vitro* cultures and human sputa (6). However,
81 the necessity to re-infect daughter cells with ϕ^2DRM limited the ability to follow isolated cells
82 over generations and study their regrowth patterns. The study also used a reporter that
83 specifically enriched for persisters of isoniazid treatment (i.e., fluorescent protein fused to the
84 *dnaK* promoter), disregarding multidrug tolerant subpopulations which are known to exist
85 within the host environment (7).
86 Here, we sought to develop a fluorescent reporter system to isolate and characterize
87 multidrug tolerant subpopulations of mycobacteria from naïve growth conditions (i.e., absence
88 of antibiotic treatment). We wanted to avoid killing susceptible cells with antibiotics in order to
89 study both persister cells *and* actively growing cells from the same culture and prevent drug
90 pressure from confounding persister formation. Instead, based on a considerable body of work
91 linking bacterial stress pathways to the acquisition of drug tolerance via translation inhibition
92 (8-13), we developed "PerSort" to enrich for translationally dormant mycobacterium (i.e., cells
93 that are able to transcribe but not translate a fluorescent reporter) under naïve conditions. We
94 demonstrated the persister-like properties of the translationally dormant subpopulation and
95 their increased abundance during stress conditions. Moreover, we performed single-cell
96 transcriptional profiling of "PerSorted" cells and highlight various mechanisms that generate
97 translationally dormant mycobacteria. Finally, using these mechanistic insights we revealed a
98 physiological response common to persister cells and demonstrated that activating respiration
99 potentiated both isoniazid and rifampicin to rapidly clear mycobacteria. Importantly, this was
100 achieved from a host-relevant condition that fosters multidrug tolerant mycobacteria. This
101 study confirms that PerSort enables a better understanding of mycobacterial phenotypic
102 heterogeneity and can lead to new strategies for shortening TB treatment.
103
104 **Results**
105
106 **Multidrug tolerant mycobacteria increase in nutrient starved conditions and show lag-**
107 **dormancy**
108 To establish a system that enriches for multidrug tolerant mycobacteria, we grew *M.*
109 *smegmatis* (MSM) in nutrient rich (7H9 media, 0.2% glycerol, 0.05% Tween-80, and ADC
110 complementation) and nutrient starved (PBS and 0.05% Tween-80) conditions. Deprivation of

111 nutrients results in a marked slowing of mycobacterial growth and concurrent phenotypic
112 tolerance to various antibiotics, including isoniazid (INH) and rifampicin (RIF) (14, 15).
113 Moreover, studies have established the relevance of the bacterial physiological state adopted
114 under nutrient starved conditions to TB infection (16). We incubated wild type MSM mc^2155
115 strain in nutrient rich or nutrient starved conditions for 12 hours (h) then treated with either 5x
116 minimum inhibitory concentration (MIC) INH or RIF (40 and 15 µg/mL respectively). Antibiotic-
117 treated MSM cultures were diluted and plated over a 20 h interval. Percent survival was
118 calculated, in reference to time 0 h, and used to generate kill curves (**Figure 1a, 1b**). According
119 to the bimodal model of bacterial persistence (17), multiple subpopulations were identified,
120 either drug susceptible or drug tolerant, as distinguished by varying slopes of killing. We further
121 estimated the abundance of drug tolerant subpopulations in either nutrient rich or nutrient
122 starved conditions via the intersection of the y-axis with the extrapolated slope of the drug
123 tolerant subpopulation. Thus, MSM cultures grown in standard conditions (i.e., nutrient rich)
124 were ~45% tolerant to INH and ~30% tolerant to RIF. Whereas after nutrient starvation, the
125 proportion of the drug tolerant subpopulations increased to ~75% for INH and ~50% for RIF.
126 The increase in delay of RIF killing under nutrient starved conditions, might reflect cell wall
127 alterations that are required for adaptation to nutrient deprivation, but also restrict entry of RIF
128 (18, 19).
129 Another advantage of the nutrient deprivation model for enriching and characterizing
130 multidrug tolerant mycobacteria is that nutrient starved bacteria can easily grow upon being
131 returned to nutrient rich media, thus this model allows easy quantification of drug susceptibility
132 and growth patterns. We characterized the population wide growth characteristics of the
133 nutrient rich and nutrient starved cultures using ScanLag, a technique that combines cell plating
134 with high-throughput imaging (20). Following 12 h incubation in nutrient rich or nutrient
135 starved conditions, MSM mc^2155 cultures were plated onto nutrient rich plates (7H10 media,
136 0.2% glycerol, OADC) and observed for colony growth by imaging at 1 h intervals. The mean
137 time of appearance (TOA) of individual colony forming units (CFUs) from the nutrient rich
138 conditions was determined to be 37 h, whereas the TOA from the nutrient starved conditions
139 was 41 h (**Figure 1c**). This significant delay in resuming growth is due to a greater abundance of
140 cells with lag-dormancy, a phenotype well-established with drug tolerance (21, 22), which
141 explains why nutrient deprived mycobacteria are multidrug tolerant.
142
143 **PerSort isolates translationally dormant mycobacteria that are multidrug tolerant**
144
145 To further characterize multidrug tolerant subpopulations, we developed a FACS-based
146 protocol to isolate translationally dormant mycobacterial cells. In drug tolerance inducing
147 conditions, translation is repressed via various mechanisms that downregulate rRNA (e.g. RelA
148 and CarD) or degrade rRNA (e.g. VapC and other toxins) [10-15]. Therefore, we hypothesized

149 that a fluorescent reporter that relays translation activity could efficiently sort and isolate drug
150 tolerant mycobacterium that form in a multitude of ways. The reporter plasmid (Trans-mEos2,
151 **Figure S1**) was constructed by inserting the highly stable fluorescent gene, *mEos2*, under the
152 transcriptional control of an anhydrotetracycline (ATc)-inducible promoter and a strong
153 mycobacterial translation initiation sequence (Shine-Dalgarno sequence), then inserted into the
154 PstKi plasmid (23-25). The PstKi plasmid contains an integrase gene and thus eliminates copy
155 number variability among cells by integrating into the mycobacterium genome. Moreover, the
156 ATc-inducible promoter achieves detectable fluorescence from a genome-integrated reporter
157 while also allowing for modulation of reporter expression.

158 The Trans-mEos2 plasmid was transformed into wild type MSM (creating the MSM-
159 mEos2 strain) for differentiation of mEos2 fluorescence levels in mycobacterial cells using FACS.
160 To minimize clumps, MSM-mEos2 cultures (grown in 7H9, 0.2% glycerol, 0.05% Tween-80, ADC
161 complementation and high shaking conditions) were passed through a 10 µm filter before
162 running on the BD FACS Influx instrument. Parameters for single-cells were defined by 3 µm
163 rainbow fluorescent beads and the efficiency of single-cell sorting was assessed using a mixed
164 culture of ATc-induced MSM-mEos2 cells (resistant to kanamycin) and MSM cells expressing
165 mCherry (resistant to hygromycin) (26). Cells from the mixed fluorescent reporter cultures were
166 sorted and plated onto 7H10 plates with appropriate antibiotic selection. Sorting was found to
167 be 93% efficient (**Figure S2**).

168 Sort gates were defined for cultivable and non-cultivable cells (*i.e.*, dead cells and viable
169 but non-culturable cells). Viable but non-culturable cells (VBNCs) are antibiotic tolerant, but
170 they lack the ability to regain active growth in standard conditions and therefore do not
171 contribute to bacteria survival (27). To exclude non-cultivable cells, MSM-mEos2 cultures were
172 stained with propidium iodide (PI) and PI signal was used for gate selection. Heat-killed cultures
173 were used for evidence of non-culturable cells in the PI(+) gate (**Figure S3)**. Gates for
174 translationally active and dormant cells were defined based on mEos2 fluorescence signal in the
175 PI(-) cultivable population (**Figure 2a**). Wild type MSM and MSM-mEos2 cultures were grown in
176 the presence of ATc (500 ng/mL) for 12 h and stained with 0.5% PI. Background fluorescence
177 from wild type MSM cells was used to define the gate for translationally dormant cells ("dim").
178 For clear distinction between subpopulations, gates were set at a higher mEoS2 fluorescence
179 signal to define MSM-mEos2 translationally active cells ("lit"), leaving ~25% of PI(-) cells
180 unselected (**Figure 2a**). Further, the PI signal gates were set such that thresholds for selection of
181 cultivable cells, PI(-), decreased with the mEos2 signal, as VBNCs were expected at high
182 proportions in low mEos2 signal range. Based on these FACS gates and following ATc-induction
183 of MSM-mEos2 cultures in standard 7H9 media (*i.e.*, same as nutrient rich conditions) for 12 h
184 (OD600 > 1) , a majority of cells were translationally active "lit" cells, while a consistent
185 subpopulation of translationally dormant "dim" cells was also present, reaching about 1% of
186 the population (**Figure 2a**). We sorted equal number of cells from the dim, lit, and PI(+) gates

187 and plated onto 7H10 media (**Figure 2b**). All of the cells from the dim and lit subpopulations
188 formed CFUs, whereas only 25% formed CFUs from the PI(+) subpopulation, confirming cells
189 from the PI(-) negative (i.e., dim and lit) gates were cultivable and devoid of VBNCs and dead
190 cells. Finally, we measured dim cell proportions following ATc-induction of MSM-mEos2
191 cultures in standard growth conditions until cultures were either in exponential (~6 h after ATc
192 addition) or stationary (12 h after ATc addition) phase of growth. Dim cells were found in low
193 numbers (~0.4% of population) during exponential phase and increased during stationary phase
194 to make up ~1% of the population (**Figure S4**). This indicates that dim cells pre-exist under low
195 stress conditions (i.e., exponential phase) and a density-dependent increase in dim cell
196 formation, likely caused by nutrient depletion of the culture during stationary phase (28).
197 Having developed the fluorescent reporter system and optimized the FACS procedure to
198 sort translationally active and dormant cells from naïve growth conditions (i.e., absence of
199 antibiotic treatment), we investigated the growth characteristics and drug susceptibility of the
200 dim and lit subpopulations. For growth characterization, cells were sorted from the PI(-) gate of
201 ATc-induced MSM-mEos2 cultures and ScanLag analysis was performed as described previously
202 (**Figure 2c**). The dim cells showed a longer TOA compared to lit cells, with a difference between
203 the subpopulations (~200 minutes) similar to that observed between nutrient rich and nutrient
204 starved cultures (**Figure 1c**). As expected, cells from the unselected PI(-) gate had a mean TOA
205 in between the dim and lit subpopulations, suggesting it is almost an equal mixture of
206 translationally active and inactive cells. To assess drug susceptibility, 100,000 dim and lit cells
207 from ATc-induced MSM-mEos2 cultures were sorted into 7H9 media containing either 5x MIC
208 INH or 5x MIC RIF. The survival of dim and lit subpopulations was determined by comparing
209 CFUs after 12 h INH or 8 h RIF treatment to CFUs before drug treatment (**Figure 2d, 2e**). The
210 drug treatment times were selected from the slowed phase of killing from the biphasic kill
211 curves (**Figure 1a, 1b**). A significantly larger percentage of dim cells survived both INH (p-value =
212 0.001) and RIF treatment (p-value = 0.006), indicating the dim cells are a multidrug tolerant
213 subpopulation. Further, the survival of dim cells was compared to the entire population of ATc-
214 induced MSM-mEos2 cultures (i.e., unsorted) grown in either nutrient rich or nutrient starved
215 conditions. The percentage of dim cells surviving INH and RIF treatment matched closely with
216 the nutrient starved cultures. These results reveal the striking similarities, both in terms of
217 growth characteristics (i.e., lag-dormancy) and antibiotic susceptibility (i.e., multidrug
218 tolerance), between dim cells and nutrient starved cultures. As such, we hypothesized the dim
219 cells are a phenotypically heterogeneous subpopulation, with translational dormancy and
220 multidrug tolerance, that increase in proportion under nutrient deprivation because their
221 physiological state is best suited to withstand such environmental stress.
222

223 **Translationally dormant mycobacteria form at different probabilities in naïve versus nutrient**
224 **starved conditions**
225
226 We used the demonstrated capability of PerSort to isolate persister-like mycobacterial
227 cells to investigate the population structure and regrowth characteristics of subpopulations
228 from both naïve (i.e., absence of antibiotic treatment) and nutrient starved conditions.
229 Following ATc induction of the MSM-mEos2 culture for 12 h, 100,000 dim and lit cells were
230 PerSorted into standard 7H9 media. Sorted samples were grown to an OD600 of 0.6, induced
231 with ATc again for 12 h and reanalyzed by FACS. Cultures generated from both dim and lit
232 subpopulations had similar structure as the parent population vis-à-vis proportions of dim and
233 lit cells (**Figure 3a**). These results demonstrate that translational dormancy of dim cells is not
234 heritable and dim and lit cells interconvert under standard *in vitro* growth conditions. We
235 further assessed regrowth by measuring OD600 over time after PerSorting 100,000 dim and lit
236 cells into standard 7H9 media. As expected, dim cell cultures grew after a longer lag phase than
237 lit cells (**Figure 3b**), but the subpopulations reached similar maximum growth rate and carrying
238 capacity (**Figure 3c**). This demonstrates that dim cells can resume normal growth (*i.e.*, same as
239 lit cells) in low stress conditions, which is a key characteristic of persister cells (29). Further,
240 ATc-induced MSM-mEos2 cultures were grown in either naïve or nutrient starved conditions
241 and then PerSorted to determine the population structure. Both dim and lit cells were present
242 in the nutrient starved cultures, but there was a significant increase in the proportion of dim
243 cells (**Figure 3d**). This confirmed our hypothesis, establishing that dim cells (i.e., translationally
244 dormant mycobacteria) dramatically increase in proportion upon nutrient starvation, further
245 suggesting that the likelihood of generating a dim cell in each cell division is distinct under low
246 stress versus high stress conditions (**Figure 3e**). Whereas dim cells (and likely other
247 phenotypically heterogeneous subpopulations) form at low probability under naïve conditions,
248 nutrient deprivation favors the formation of dim cells (a translationally dormant and multidrug
249 tolerant subpopulation) and enables mycobacteria to withstand stress, including drug
250 treatment.
251
252 **Translationally dormant mycobacteria are composed of three discernable subtypes of**
253 ***vapC30*, *mazF* toxins and(or) *relA/spoT* over-expressing cells**
254
255 To further characterize the formation of phenotypically heterogeneous mycobacteria,
256 we profiled within individual cells of both dim and lit subpopulations following PerSort, the
257 transcript levels of 45 genes that were previously implicated in persister formation and drug
258 tolerance in *Mycobacterium* spp. and *E. coli* (**Table S1**). Single-cell gene expression profiling was
259 performed with the Fluidigm Biomark 48x48 system per manufacturer instructions and assayed
260 relative to single-cell genomic DNA signal. The DNA signal from single dim and lit cells was

261 found to have low variation in expression (**Figure S5a**), indicating that transcripts per genome
262 copy accurately reports differential gene expression. Transcript abundances were normalized to
263 a spike-in RNA control to account for experimental noise (**Figure S5b**).
264 Kernel PCA (kPCA) with radial basis function identified distinct clusters consisting of dim
265 and lit cells as well as some overlap between the subpopulations (**Figure S6**). The overlap could
266 indicate some phenotypic uncertainty, based on the expression of selected persister genes. We
267 used a tree-based feature selection (see *Methods*) to rank the persister genes for their ability to
268 differentiate the dim and lit subpopulations (30). Using the top features (**Table S2**), we
269 performed unsupervised hierarchical clustering and dynamic tree cutting to identify four
270 distinct clusters within the dim cells (**Figure 4a**) (31, 32). Specifically, clustering revealed
271 subtypes of translationally dormant mycobacteria with high *relA/spoT*, *vapC30*, or *mazF*
272 expression (and another subtype with no distinct signature of persister gene expression).
273 Importantly, similar clustering analysis did not detect any statistically significant subtypes
274 within the lit cells (**Figure 4a**). Increased expression of *relA/spoT* was observed in higher
275 proportions of dim cells, compared to lit cells. The bifunctional activity of the protein (*i.e.*,
276 hydrolase and synthase) (33) could suggest different functions of RelA/SpoT between the dim
277 and lit subpopulations.
278 We sought further evidence that one or some combination of the three gene features
279 identified from single-cell expression profiling (i.e., RelA/SpoT, VapC30, or MazF) were active in
280 the dim cell subpopulation. The VapC30 and MazF toxins belong to a family of type II toxin-
281 antitoxin (TA) systems, implicated in mycobacterial dormancy and persistence (28, 34, 35).
282 Activation of the type II TA system results in toxin-mediated cleavage of tRNAs (36), or rRNAs
283 (12, 36) causing translational dormancy (37). We analyzed 16S and 23S rRNA levels in dim and
284 lit cells by qRT-PCR. We discovered that indeed dim cells have lower rRNA content relative to lit
285 cells (**Figure 4b**, 16s rRNA log2 normalized FC = -4.17, 23s rRNA log2 normalized FC = -2.34).
286 There was no discernible decrease in transcript level of a highly expressed metabolic gene
287 (**Figure 4b**, phosphoglucoisomerase log2 FC = -0.87). These results support the notion that
288 some of the translationally dormant mycobacteria are formed via toxin-mediated cleavage of
289 rRNA.
290
291 **Translationally dormant mycobacteria are in a low O_2 respiratory state**
292
293 The single-cell expression data revealed that translationally dormant mycobacteria may
294 be formed by at least three distinct mechanisms. The multiplicity of mechanisms confers
295 robustness to the pathogen, but also thwarts therapeutic strategies to block formation of the
296 multidrug tolerant mycobacteria. Nonetheless, we found evidence from literature that the
297 mechanisms for persister formation converge on a common physiology and predicted the dim
298 cells are in a reduced state of respiration. Direct measurements of respiration rate (e.g., oxygen

electrode or Seahorse analysis) are problematic with low bacterial cell numbers. Therefore, to test whether dim cells have lower O_2 metabolism we measured reactive oxygen species (ROS) levels in single-cells from the PerSorted dim and lit subpopulations using CellRox-orange. It is established that increases in ROS levels are linked with increased flux to the TCA cycle and oxidative metabolism (38, 39). Cultures of ATc-induced MSM-mEos2 were grown in standard 7H9 media, stained with CellRox-orange (40), and PerSorted to compare ROS levels between dim and lit cells (**Figure 4c**). As reference controls, MSM-mEos2 cultures were treated with Mn-TBAP (ROS inducer) or N-acetyl-cysteine (ROS quencher) with Mn-TBAP. Cultures were incubated in CellRox-orange stain for 1.5 h to ensure uniform dye permeation across the subpopulations. The ROS levels were significantly lower in dim cells (**Figure 4c**), confirming the translationally dormant mycobacteria have reduced oxidative metabolism.

Activation of oxidative metabolism eliminates translationally dormant mycobacteria and achieves faster killing by INH and RIF in nutrient starved conditions

Since respiration may play an important role in generating and/or maintaining translationally dormant mycobacteria, we explored the use of L-cysteine to activate oxidative metabolism and reduce the proportion of dim cells. It is well-known that exogenous amino acids fuel the TCA cycle and oxidative respiration in bacteria, especially molecules such as cysteine and proline which are rapidly metabolized (41). Cultures of MSM-mEos2 were grown in standard 7H9 media with 4mM L-cysteine (similar growth observed in 7H9 media with or without 4 mM L-cysteine, data not shown), induced with ATc and PerSorted for dim and lit subpopulations. The L-cysteine treated MSM-mEos2 cultures were found to be completely devoid of dim cells (**Figure 5a)**. Further, we supplemented nutrient starved MSM cultures with 4 mM L-cysteine and then treated with either 5x MIC INH or 5x MIC RIF. Kill-curves for the antibiotic and L-cysteine treated cultures were generated as previously described (**Figure 5b, c**). Activation of respiration by adding L-cysteine to nutrient starved cultures potentiated clearance by INH and RIF at rates identical to or better than rates for nutrient rich cultures. This further corroborates that, similar to dim cells, the expanded translationally dormant mycobacteria in nutrient starved conditions share a low respiratory physiologic state. Ultimately, these results demonstrate that drug adjuvants that activate respiration could shorten drug treatment, particularly in environmental niches that foster drug tolerance in mycobacteria.

Discussion

The ability of microorganisms to survive sudden environmental changes stems from the formation of phenotypically heterogeneous subpopulations. Phenotypic heterogeneity confers fitness advantage to clonal microbial communities, such as infectious MTB, but impedes efforts

337 of the immune system to clear the pathogen as well as chemotherapeutic efforts to rapidly
338 treat TB. In this study, we developed a method to identify and characterize multidrug tolerant
339 subpopulations of mycobacterium cells. We demonstrated that our method enables a better
340 understanding of phenotypic heterogeneity in mycobacteria in naïve and stressed conditions,
341 and could lead towards novel strategies to shorten TB treatment.

342 We generated a fluorescent reporter system, PerSort, which sorts mycobacterial cells
343 based on translational activity. We found a small proportion of translationally dormant ("dim")
344 cells from naïve cultures, in the absence of stress such as antibiotic treatment. We confirmed
345 the translationally dormant subpopulation was tolerant to both INH and RIF, demonstrated a
346 longer lag phase upon regrowth, and could regenerate the original population structure upon
347 regrowth (i.e., a mixture of translationally active and dormant cells). These data indicate the
348 translationally dormant subpopulation identified by PerSort consist of cells with properties of
349 persisters. We report these cells pre-exist in low numbers in an isogenic MSM culture growing
350 without stress and exponential phase of growth. The translationally dormant subpopulation
351 (along with other phenotypically heterogeneous subpopulations) is generated stochastically, as
352 a bet-hedging strategy, for the mycobacterial population to withstand unpredictable
353 environmental stress.

354 Indeed, we discovered an increase in the proportion of the translationally dormant
355 subpopulation under density-dependent stress, and even more so under nutrient starvation.
356 This suggests an environmentally induced component that forms this subpopulation, in addition
357 to stochastic formation. It also begs the question of what is influencing the translational state of
358 this mycobacterial subpopulation. The PerSort method overcomes the challenge of
359 characterizing persisters at single cell resolution by sorting them and, importantly, not killing
360 the susceptible cells with antibiotics. This technological advancement has overcome the
361 confounding issue that antibiotic treatment itself induces persister cell formation (42, 43) and
362 allows comparative analysis of persister cells *and* actively growing drug susceptible cells from
363 the *same* culture. Because of these novel capabilities of PerSort, we were able to quantify
364 transcript abundance of 45 genes associated with persister formation and drug tolerance in
365 single-cells from both the translationally dormant (i.e., dim) and translationally active (i.e., lit)
366 subpopulations. Expression analysis revealed that translationally dormant persisters are a mix
367 of *vapC30*, *mazF*, and *relA/spoT* overexpressing cells. These results reinforce the hypothesis
368 that there are multiple pathways (both stochastically and deterministically activated) to
369 become a persister cell and reveals the complex and combinatorial schemes used by
370 mycobacteria to generate heterogeneous subpopulations.

371 Within the translationally dormant cells, we found that high expression of toxin *mazF*
372 was also associated with high *relA/spoT* expression. We suspect that *mazEF* could be regulated
373 by the alarmone response, elicited by RelA/SpoT synthesis of (p)ppGpp, in a manner that is
374 induced deterministically by stress conditions (44). In contrast, the single-cell expression data

375 suggest that *vapC30* overexpression can also act to induce persister formation, in a
376 spontaneous and alarmone-independent manner. This supports a recent study demonstrating
377 that a *relA/spoT* knockout mutant of MSM, with reduced alarmone response, still formed
378 persisters at levels similar to wildtype (45). This collection of evidence points toward multiple
379 mechanisms of generating the translationally dormant mycobacteria characterized here, some
380 of which are deterministically activated (controlled by *relA/spoT* in response to stress) and
381 some of which are stochastically activated (controlled by spontaneous *vapC30* activation) (46).
382 While MSM has a single VapBC-type TA system, MTB has 70 copies of VapBC (35), indicating the
383 human pathogen has evolved to increase phenotypic diversity and bet-hedging for survival in
384 the host environment. Much work is still needed, specifically using live cell monitoring
385 techniques, to understand how and when these TA systems are activated to form persisters,
386 and the contribution of other mechanisms, either stochastic or deterministic, to phenotypic
387 heterogeneity in MTB.
388 The activation of TA systems (47) and the alarmone response (48) has been shown to
389 decrease oxidative metabolism in bacterial persisters. Moreover, it is expected that
390 translational dormancy would be associated with low respiration (28). Given this knowledge,
391 we demonstrated lower ROS levels in the translationally dormant subpopulation compared to
392 translationally active cells, indicating reduced oxygen metabolism in the persister cells. In other
393 words, regardless of their mechanism of formation (i.e., *vapC30*, *mazF*, or *relA/spoT*
394 overexpression), the persister subpopulation shares a low oxygen respiratory state, which
395 presents a vulnerability that could be targeted to modulate this subpopulation (**Figure 6**). We
396 confirmed that addition of L-cysteine, which is known to activate oxidative metabolism (49),
397 dramatically reduced the proportion of translationally dormant cells in nutrient starved MSM
398 cultures, conditions where the population is abundant. This goes beyond previous studies by
399 directly demonstrating that promoting oxidative metabolism reduces the proportion of
400 multidrug tolerant persister cells that form independent of drug pressure. Furthermore, the
401 addition of L-cysteine was able to effect complete clearance by INH and RIF in nutrient starved
402 conditions. The addition of L-cysteine potentiates faster drug killing by converting (or limiting
403 the formation of) multidrug tolerant persister cells, cells with enhanced fitness advantage in the
404 host-relevant stress (nutrient starved) conditions, to a population with increased oxidative
405 metabolism and drug susceptibility. Our findings prove that until properties of heterogeneous
406 subpopulations are disrupted, we will not be able to successfully clear mycobacterial cells in
407 infected patients. This study highlights how novel methods to isolate and characterize
408 heterogeneous subpopulations can enable targeted strategies to eliminate detrimental
409 persister cells, and thereby shorten the course of treatment.
410
411 **Materials and Methods**
412

413 **Bacterial growth and MSM-mEos2 strain development**. *Mycobacterium smegmatis* mc^2155
414 strain (MSM) was obtained from ATCC and grown in 7H9 broth medium (Difco) with 0.2%
415 glycerol, 0.05% Tween-80, and 10% ADC enrichment (BD biosciences). pSTKi-mEos2 plasmid
416 was constructed from pSTKi plasmid and pRSETa mEos2 plasmid (23, 25). Synthetic oligo with
417 translation initiation signal (mycoSD) was used to amplify mEos2 from pRSETa mEos2 plasmid,
418 and amplified fragment was inserted into the pSTKi plasmid with restriction ligation at BamH1
419 and EcoR1 sites. The pSTKi-mEos2 transcript was electroporated into electrocompetent MSM
420 cultures, transformed colonies were selected on 7H10 plates with 30 µg/ml kanamycin (KAN).
421 MSM-mEos2 cells were cultured in 7H9 media supplemented with 30 µg/ml KAN.
422
423 **Development of PerSort**. The PerSort method was developed using BD FACS Influx. A 70 micron
424 tip and sheath fluid from BD bioscience was used in sorting and FACS analysis. Green
425 fluorescent beads (3.5 micron) and 5 micron Accudrop beads from BD biosciences were used to
426 calibrate the instrument for laser alignment, compensation, and cell sorting. Propidium Iodide
427 (PI) stain (SigmaAldridge, 0.5%) was used to stain dead cells. Heat killed cells (incubated at 70° –
428 80° C for 5 mins) were used as dead cell control for PI stain. MSM cells with pCHERRY3 plasmid
429 (MSM-mCherry) (26) was used to optimize single-cell mycobacterium sorting. MSM-mEos2
430 (KAN resistant) cultures were grown to OD600 of 0.6 and induced with 500 ng/ml ATc. Induced
431 cultures were incubated at 37 ^{o} C for 12 h. MSM-mCherry (Hygromycin resistant) were mixed
432 with induced MSM-mEos2 cultures in equal proportions and single mEos2 and mCherry cells
433 were sorted and plated on 7H10 plates with Kan and Hyg to determine the efficiency of single-
434 cell sorting (**Figure S2**). Gates for sorting dim and lit cells of ATc induced MSM-mEos2 strains
435 (induced for 12 h) were determined using uninduced MSM-mEos2 strains stained with PI. FACS
436 data was analyzed in FlowJo software (ver. 10).
437
438 **Antimicrobial tolerance assay**. Minimum inhibitory concentrations (MIC) of the MSM-mEOS2
439 strains were determined with disk diffusion assay (50). To determine percent survival, cultures
440 (bulk and PerSorted) were incubated in 7H9 media containing desired MIC concentrations of
441 INH and RIF. Drug treated bacteria were washed with or diluted (1:100) in 7H9 media and
442 plated (100 µl) or spotted (5 µl) on 7H10 media with 30 µg/ml KAN at time points 0, 8, 12, 16,
443 20, and 24 h after incubation. Percentage survival was calculated with respect to 0 h.
444
445 **qRT-PCR of PerSorted samples.** Dim and lit cells were sorted into 500 µl TriZol and RNA was
446 extracted with DirectZol RNA purification kit (Zymo Research) with the manufacturer's
447 instructions. qRTPCR was performed with primers mentioned in **Table S3** with Luna® Universal
448 Probe One-Step RT-qPCR Kit (New England Biolabs). Log2 normalized RNA abundances were
449 calculated using ValidPrime signal as reference (51).
450
451 **Single-cell persister gene expression and analysis**. The Fluidigm Biomark system with 48x48
452 plates was used for this study. Single dim and lit cells were PerSorted into 96 well plates with
453 VILO™ reaction mix (5x), SUPERase (Invitrogen™), and 10% NP40 in a pre-noted random order
454 to avoid sampling bias. Sorted plates were spun down and freeze-thawed 3 times on dry ice to
455 rupture cells. ValidPrime assay (51) for non-transcribed genomic DNA was used to determine
456 the rupture efficiency and calculate the signal from a single nucleic-acid strand (used as

457 reference to calculate transcript abundance). Reverse transcription (RT) was performed on
458 freeze thawed cells with VILO cDNA preparation mixture, T4-Gene32 protein, and random
459 hexamer primers. RNA spike-in (ECC2_SpikeIn RNA, 10 pM) was included in the RT master mix.
460 cDNA of the genes of interest (**Table S1**) was pre-amplified with TaqMan® PreAmp master mix
461 (Invitrogen™) and equimolar mixture of forward and reverse strand primers designed for the
462 genes of interest (**Table S3**). Primers were removed with Exonuclease I (Invitrogen™). Primers
463 sets used for preamplification were primed into the 48x48 Biomark assay plates. Quantitative
464 PCR assay with Biomark prescribed protocol was run on diluted, pre-amplified Exo 1 treated
465 cDNA with Sso Fast EvaGreen Supermix (Bio-Rad laboratories). Quality control for determining,
466 sorting, cell lysis, and cDNA preparation was performed by comparing the CT values of genomic
467 DNA control and spike-in control in all the cells (**Figure S5a,b**). Expression levels of genes was
468 measured as ∂CT in individual cells with reference to genomic DNA control (expected to result
469 from 1 copy of genomic DNA), less than or equal expression (of genomic DNA control) was
470 considered as zero expression and assays with CT >40 were flagged as missing values. ∂CT
471 values for each cells were corrected by adding or subtracting the deviation from median ∂CT of
472 spike-in control for a particular cell. Hierarchical clustering was performed with Python Seaborn
473 package and the R package, PVclust.
474
475 **Feature selection of single-cell clusters**. Ratio of toxin expression to their respective antitoxin
476 expression was calculated and included along with the other persister gene expression values.
477 Key features that differentiate dim and lit subpopulations were selected with tree-based
478 feature selection tool (30). Weights of the features that signify its ability to differentiate
479 between dim and lit sub populations were estimated as an average over 100 iterations of
480 randomly selected subsets of the dataset (70% of gene expression values). Constraints of gene
481 regulation was also used in selection of features as most persisters specific responses are a part
482 of alarmone response, a broad, genome wide change in transcript levels (52). The three
483 features with the highest weights and evidence of additional criteria were selected for
484 identification of clusters within dim and lit cells.
485
486 **In situ ROS level measurements with CellRox assay**. MSM-mEos2 cells were induced with ATc
487 (500 ng/ml) and incubated for 12 h under standard growth conditions. 10 µM N-acetyl cysteine
488 (NAC), an oxidative agent that reduces level of in situ reactive oxygen species (ROS) was added
489 to the induced MSM-mEos2 cultures and incubated at 37° C for 90 mins to prepare the negative
490 control. Along with negative control, another set of induced cultures were treated with a ROS
491 inducing 100µM MnTBAP (Sigma Aldrich, 55266-18-7) and incubated for 15 mins to prepare
492 positive control. CellRox orange (Thermo Fisher, C10443), was added to the induced samples
493 and control and incubated for 30 mins at room temperature. FACS analysis was performed to
494 measure the CellROX orange intensity. ROS + and negative gates were determined with control
495 samples and ROS levels in dim and lit cell population were determined with reference to the
496 controls.
497
498 **Dim cell proportion and antimicrobial tolerance following L-cysteine addition**. MSM-mEos2
499 cells were grown in PBS and 0.05% Tween-80, with and without 4mM L-cysteine, to an OD600
500 of 0.6. Cultures were induced with ATc (500 ng/ml) and incubated for 12 h. Dim cell proportions

501 in both conditions were measured with PerSort assay and normalized to the dim cell
502 proportions observed in optimal growth conditions (growth in 7H9 media without L-cysteine).
503 Tolerance of cultures grown in various conditions was measured with time kill curve assays,
504 under 5x MIC RIF (17.5 µg/ml) and 5x MIC INH (20 µg/ml) treatment. The % survival was
505 measured at varying time point by counting number of CFUs on 7H10 plates in reference to the
506 time point 0 of the respective samples.
507
508
509

Acknowledgements: We thank members of the Baliga lab for critical discussions; Amardeep Kaur for her technical expertise; Tim Petersen and Monica Orellana for help with FACS. Funding was provided by the National Institute of Allergy and Infectious Diseases of the National Institutes of Health [R01AI128215] and [U19AI10676, U19AI135976]; and National Science Foundation [1518261, 1565166, and 1616955].

Author contributions: V.S. designed research, performed experiments, analyzed data and wrote the paper. M.L.A-O. performed computational analyses. E.J.R.P and N.S.B. designed research, analyzed data, and wrote the paper.

Competing interests: The authors declare no competing financial interests.

References

1. Philippi T, Seger J. Hedging one's evolutionary bets, revisited. Trends Ecol Evol. 1989;4(2):41-4.
2. CARE T. International Standards for Tuberculosis Care. TB CARE I. The Hague, The Netherlands2014.
3. Sarathy JP, Via LE, Weiner D, Blanc L, Boshoff H, Eugenin EA, et al. Extreme Drug Tolerance of Mycobacterium tuberculosis in Caseum. Antimicrob Agents Chemother. 2018;62(2).
4. Chaulk CP, Kazandjian VA. Directly observed therapy for treatment completion of pulmonary tuberculosis: Consensus Statement of the Public Health Tuberculosis Guidelines Panel. JAMA. 1998;279(12):943-8.
5. Manina G, Dhar N, McKinney JD. Stress and host immunity amplify Mycobacterium tuberculosis phenotypic heterogeneity and induce nongrowing metabolically active forms. Cell Host Microbe. 2015;17(1):32-46.
6. Jain P, Weinrick BC, Kalivoda EJ, Yang H, Munsamy V, Vilcheze C, et al. Dual-Reporter Mycobacteriophages (Phi2DRMs) Reveal Preexisting Mycobacterium tuberculosis Persistent Cells in Human Sputum. MBio. 2016;7(5).
7. Liu Y, Tan S, Huang L, Abramovitch RB, Rohde KH, Zimmerman MD, et al. Immune activation of the host cell induces drug tolerance in Mycobacterium tuberculosis both in vitro and in vivo. J Exp Med. 2016;213(5):809-25.
8. Cho J, Rogers J, Kearns M, Leslie M, Hartson SD, Wilson KS. Escherichia coli persister cells suppress translation by selectively disassembling and degrading their ribosomes. Mol Microbiol. 2015;95(2):352-64.
9. Shah D, Zhang Z, Khodursky A, Kaldalu N, Kurg K, Lewis K. Persisters: a distinct physiological state of E. coli. BMC Microbiol. 2006;6:53.
10. Torrey HL, Keren I, Via LE, Lee JS, Lewis K. High Persister Mutants in Mycobacterium tuberculosis. PLoS One. 2016;11(5):e0155127.
11. Ahidjo BA, Kuhnert D, McKenzie JL, Machowski EE, Gordhan BG, Arcus V, et al. VapC toxins from Mycobacterium tuberculosis are ribonucleases that differentially inhibit growth and are neutralized by cognate VapB antitoxins. PLoS One. 2011;6(6):e21738.

552 12. Schifano JM, Edifor R, Sharp JD, Ouyang M, Konkimalla A, Husson RN, et al.
553 Mycobacterial toxin MazF-mt6 inhibits translation through cleavage of 23S rRNA at the
554 ribosomal A site. Proc Natl Acad Sci U S A. 2013;110(21):8501-6.
555 13. Stallings CL, Stephanou NC, Chu L, Hochschild A, Nickels BE, Glickman MS. CarD is an
556 essential regulator of rRNA transcription required for Mycobacterium tuberculosis persistence.
557 Cell. 2009;138(1):146-59.
558 14. Betts JC, Lukey PT, Robb LC, McAdam RA, Duncan K. Evaluation of a nutrient starvation
559 model of Mycobacterium tuberculosis persistence by gene and protein expression profiling.
560 Mol Microbiol. 2002;43(3):717-31.
561 15. Xie Z, Siddiqi N, Rubin EJ. Differential antibiotic susceptibilities of starved
562 Mycobacterium tuberculosis isolates. Antimicrob Agents Chemother. 2005;49(11):4778-80.
563 16. McKinney JD, Honer zu Bentrup K, Munoz-Elias EJ, Miczak A, Chen B, Chan WT, et al.
564 Persistence of Mycobacterium tuberculosis in macrophages and mice requires the glyoxylate
565 shunt enzyme isocitrate lyase. Nature. 2000;406(6797):735-8.
566 17. Balaban NQ, Merrin J, Chait R, Kowalik L, Leibler S. Bacterial persistence as a phenotypic
567 switch. Science. 2004;305(5690):1622-5.
568 18. Sebastian JS, S., Ajitkumar, P. Reduced Permeability to Rifampicin by Capsular
569 Thickening as a Mechanism of Antibiotic Persistence in Mycobacterium tuberculosis. BioRxiv.
570 2019;624569.
571 19. McNeil MBC, S.; Awasthi, D.; Parish, T. Cell wall inhibitors increase the accumulation of
572 rifampicin in Mycobacterium tuberculosis. Access Microbiology. 2019;1.
573 20. Levin-Reisman I, Fridman O, Balaban NQ. ScanLag: high-throughput quantification of
574 colony growth and lag time. J Vis Exp. 2014(89).
575 21. Levin-Reisman I, Ronin I, Gefen O, Braniss I, Shoresh N, Balaban NQ. Antibiotic tolerance
576 facilitates the evolution of resistance. Science. 2017;355(6327):826-30.
577 22. Fridman O, Goldberg A, Ronin I, Shoresh N, Balaban NQ. Optimization of lag time
578 underlies antibiotic tolerance in evolved bacterial populations. Nature. 2014;513(7518):418-21.
579 23. McKinney SA, Murphy CS, Hazelwood KL, Davidson MW, Looger LL. A bright and
580 photostable photoconvertible fluorescent protein. Nat Methods. 2009;6(2):131-3.
581 24. Sawyer EB, Grabowska AD, Cortes T. Translational regulation in mycobacteria and its
582 implications for pathogenicity. Nucleic Acids Res. 2018;46(14):6950-61.
583 25. Parikh A, Kumar D, Chawla Y, Kurthkoti K, Khan S, Varshney U, et al. Development of a
584 new generation of vectors for gene expression, gene replacement, and protein-protein
585 interaction studies in mycobacteria. Appl Environ Microbiol. 2013;79(5):1718-29.
586 26. Carroll P, Schreuder LJ, Muwanguzi-Karugaba J, Wiles S, Robertson BD, Ripoll J, et al.
587 Sensitive detection of gene expression in mycobacteria under replicating and non-replicating
588 conditions using optimized far-red reporters. PLoS One. 2010;5(3):e9823.
589 27. Oliver JD. The viable but nonculturable state in bacteria. J Microbiol. 2005;43 Spec
590 No:93-100.
591 28. Keren I, Minami S, Rubin E, Lewis K. Characterization and transcriptome analysis of
592 Mycobacterium tuberculosis persisters. MBio. 2011;2(3):e00100-11.
593 29. Orman MA, Henry TC, DeCoste CJ, Brynildsen MP. Analyzing Persister Physiology with
594 Fluorescence-Activated Cell Sorting. Methods Mol Biol. 2016;1333:83-100.

595 30. Baranauskas JN, O.; Nozawa, S.; Macedo, A. A tree-based algorithm for attribute
596 selection. Applied Intelligence. 2018;48(4):821-33.
597 31. Suzuki R, Shimodaira H. Pvclust: an R package for assessing the uncertainty in
598 hierarchical clustering. Bioinformatics. 2006;22(12):1540-2.
599 32. Langfelder P, Zhang B, Horvath S. Defining clusters from a hierarchical cluster tree: the
600 Dynamic Tree Cut package for R. Bioinformatics. 2008;24(5):719-20.
601 33. Weiss LA, Stallings CL. Essential roles for Mycobacterium tuberculosis Rel beyond the
602 production of (p)ppGpp. J Bacteriol. 2013;195(24):5629-38.
603 34. Ramage HR, Connolly LE, Cox JS. Comprehensive functional analysis of Mycobacterium
604 tuberculosis toxin-antitoxin systems: implications for pathogenesis, stress responses, and
605 evolution. PLoS Genet. 2009;5(12):e1000767.
606 35. Sala A, Bordes P, Genevaux P. Multiple toxin-antitoxin systems in Mycobacterium
607 tuberculosis. Toxins (Basel). 2014;6(3):1002-20.
608 36. Winther KS, Gerdes K. Regulation of enteric vapBC transcription: induction by VapC
609 toxin dimer-breaking. Nucleic Acids Res. 2012;40(10):4347-57.
610 37. Germain E, Roghanian M, Gerdes K, Maisonneuve E. Stochastic induction of persister
611 cells by HipA through (p)ppGpp-mediated activation of mRNA endonucleases. Proc Natl Acad
612 Sci U S A. 2015;112(16):5171-6.
613 38. Ishihara H, Nakazaki M, Kanegae Y, Inukai K, Asano T, Katagiri H, et al. Effect of
614 mitochondrial and/or cytosolic glycerol 3-phosphate dehydrogenase overexpression on
615 glucose-stimulated insulin secretion from MIN6 and HIT cells. Diabetes. 1996;45(9):1238-44.
616 39. Talior I, Yarkoni M, Bashan N, Eldar-Finkelman H. Increased glucose uptake promotes
617 oxidative stress and PKC-delta activation in adipocytes of obese, insulin-resistant mice. Am J
618 Physiol Endocrinol Metab. 2003;285(2):E295-302.
619 40. Bone BS, B.; Olszowy, M. Reactive oxygen probes - a broad range of colors with easier
620 labeling and compatibility with fixation: novel CellROX reagents from Molecular Probes (P3295).
621 J Immunol. 2013;190(1 Supplement).
622 41. Zampieri M, Horl M, Hotz F, Muller NF, Sauer U. Regulatory mechanisms underlying
623 coordination of amino acid and glucose catabolism in Escherichia coli. Nat Commun.
624 2019;10(1):3354.
625 42. Kwan BW, Valenta JA, Benedik MJ, Wood TK. Arrested protein synthesis increases
626 persister-like cell formation. Antimicrob Agents Chemother. 2013;57(3):1468-73.
627 43. Dorr T, Vulic M, Lewis K. Ciprofloxacin causes persister formation by inducing the TisB
628 toxin in Escherichia coli. PLoS Biol. 2010;8(2):e1000317.
629 44. Aizenman E, Engelberg-Kulka H, Glaser G. An Escherichia coli chromosomal "addiction
630 module" regulated by guanosine [corrected] 3',5'-bispyrophosphate: a model for programmed
631 bacterial cell death. Proc Natl Acad Sci U S A. 1996;93(12):6059-63.
632 45. Bhaskar A, De Piano C, Gelman E, McKinney JD, Dhar N. Elucidating the role of (p)ppGpp
633 in mycobacterial persistence against antibiotics. IUBMB Life. 2018;70(9):836-44.
634 46. Albrethsen J, Agner J, Piersma SR, Hojrup P, Pham TV, Weldingh K, et al. Proteomic
635 profiling of Mycobacterium tuberculosis identifies nutrient-starvation-responsive toxin-
636 antitoxin systems. Mol Cell Proteomics. 2013;12(5):1180-91.

637 47. McKenzie JL, Robson J, Berney M, Smith TC, Ruthe A, Gardner PP, et al. A VapBC toxin-
638 antitoxin module is a posttranscriptional regulator of metabolic flux in mycobacteria. J
639 Bacteriol. 2012;194(9):2189-204.
640 48. Verstraeten N, Knapen WJ, Fauvart M, Michiels J. Membrane depolarization-triggered
641 responsive diversification leads to antibiotic tolerance. Microb Cell. 2015;2(8):299-301.
642 49. Vilcheze C, Hartman T, Weinrick B, Jain P, Weisbrod TR, Leung LW, et al. Enhanced
643 respiration prevents drug tolerance and drug resistance in Mycobacterium tuberculosis. Proc
644 Natl Acad Sci U S A. 2017;114(17):4495-500.
645 50. Bonev B, Hooper J, Parisot J. Principles of assessing bacterial susceptibility to antibiotics
646 using the agar diffusion method. J Antimicrob Chemother. 2008;61(6):1295-301.
647 51. Laurell H, Iacovoni JS, Abot A, Svec D, Maoret JJ, Arnal JF, et al. Correction of RT-qPCR
648 data for genomic DNA-derived signals with ValidPrime. Nucleic Acids Res. 2012;40(7):e51.
649 52. Dahl JL, Kraus CN, Boshoff HI, Doan B, Foley K, Avarbock D, et al. The role of RelMtb-
650 mediated adaptation to stationary phase in long-term persistence of Mycobacterium
651 tuberculosis in mice. Proc Natl Acad Sci U S A. 2003;100(17):10026-31.
652

653

654

655 **Figure legend**
656
657 **Figure 1:** Time-kill curves and growth characteristics of *M. smegmatis* from nutrient rich and
658 nutrient starved conditions. **a**,**b**. Time-kill curves of MSM cultures grown in nutrient rich (NR) or
659 nutrient starved (NS) conditions treated with 5x MIC INH (**a**) or 5x MIC RIF (**b**). The solid lines
660 indicate experimentally observed time-kill curves. Data points are from three experimental
661 replicates, error bars were calculated by measuring standard deviation between replicates. The
662 dashed and dotted lines distinguish the slopes of the susceptible and tolerant subpopulations,
663 respectively. **c.** ScanLag analysis showing time of appearance (TOA) of cultures grown in
664 nutrient rich and nutrient starved conditions. Error bars within the violin plot are standard
665 deviation with confidence interval of 0.9. The dashed lines indicate the mean TOA from cultures
666 grown in nutrient rich or nutrient starved conditions. Mean TOA of nutrient starved and
667 nutrient rich conditions were compared with Students-t test.
668
669 **Figure 2:** PerSort isolation and characterization of subpopulations from ATc-induced MSM-
670 mEos2 cultures. **a**. Top: Population structure of ATc-induced (500ng/ml) MSM-mEos2 cells from
671 single-cell gates, represented by mEos2 fluorescence on x-axis and propidium iodide (PI, 5µl/ml)
672 fluorescence on y-axis. Polygons indicate the gates for non-culturable cells (PI(+)), dim cells, and
673 lit cells with the proportion of cells in that particular gate. Bottom: Cumulative distribution of
674 mEos2 florescence intensity in MSM-mEos2 cells, dashed lines indicate boundaries of sort gates
675 for dim, lit, and unselected PI(-) cells. **b.** Cultivability of PerSorted dim, lit and PI(-) cells from
676 ATc-induced MSM-mEos2 cultures. The "% cultivable" was calculated from the number of CFUs
677 from 200 sorted cells. Experiments were performed in triplicates and error bars represent the
678 standard deviation between replicates. Significance of cultivability difference between dim, lit
679 and non-culturable subpopulations was calculated with Students t-test. **c.** ScanLag analysis of
680 dim, unselected PI(-) and lit cells from PerSorted MSM-mEos2 cultures induced with ATc (500
681 ng/mL), the dashed lines in the violin plot indicate mean TOA of the sorted subpopulations.
682 Error bars within the violin plot are standard deviation with confidence interval of 0.9. **d,e**. %
683 survival of 5x MIC INH or 5x MIC RIF treatment of PerSorted dim and lit cells of MSM-mEos2
684 cultures induced with ATc (500 ng/ml), compared to % survival of whole populations (i.e.,
685 unsorted) of MSM-mEos2 induced with ATc (500 ng/ml) and grown in nutrient rich and starved
686 conditions. Experiments were performed in triplicates and error bars represent the standard
687 deviation between replicates. Significance of survival between dim and lit subpopulations was
688 calculated with Students-t test.
689
690 **Figure 3:** Regrowth dynamics of PerSorted dim and lit cells and population structure under
691 naïve versus nutrient starved conditions. **a.** Dim and lit cell proportions in cultures regrown
692 from PerSorted dim and lit populations obtained from ATc-induced MSM-mEos2 cultures. The
693 proportions of cells in each subpopulation were measured from the gating methods described
694 in Figure 2a. **b,c**. Lag phase and maximum growth rate were calculated from OD600 absorbance
695 measurements of dim and lit cells PerSorted into 7H9 media. Error bars were calculated by
696 measuring standard deviation in the lag phase and maximum growth rates between dim and lit

697 cells (*n* = 100,000). Significance of differences between dim and lit subpopulations were
698 calculated with Students-t test. NS, not significant. **d**. Population structure of ATc-induced
699 MSM-mEos2 cultures grown in naïve (green) and nutrient starved (grey) conditions. **e.** A model
700 describing the formation of dim cells under naïve and nutrient starved conditions in
701 mycobacterium. The probability of dim cell formation was calculated from their relative
702 proportion in the indicated culture conditions.
703
704 **Figure 4:** Single-cell gene expression and ROS levels from PerSorted single dim and lit cells. **a**.
705 Hierarchical clustering of top ranked features in PerSorted dim and lit single-cells. Blocks in the
706 cluster represent the statistically significant clusters (p-value = 0.01). **b**. qRT-PCR measurement
707 of 16s rRNA, 23s rRNA and Phospho-glucoisomerase (PGI, MSMEG_5541) levels in PerSorted
708 dim and lit cells (*n* = 300 cells). Error bars were calculated by measuring standard deviation of
709 gene expression. P-values were calculated with Student's t-test between the dim and lit cells. **c.**
710 Reactive oxygen Species (ROS) levels, measured with CellRox, of ATc-induced MSM-mEos2
711 cultures grown in nutrient rich conditions and PerSorted into dim and lit subpopulations. ROS
712 was quenched with N-acetyl cysteine and induced with MnTBAP and used as reference
713 controls. Significance of ROS levels between dim and lib subpopulations was calculated by K-S
714 test (K-S statistics of CellRox orange intensity between dim and lit population; K-S max
715 Difference: 56.1%, K-S max at Intensity: 14.8551, K-S probability: >99.9%).
716
717 **Figure 5:** Dim cell proportion and time-kill curves upon L-cysteine addition to nutrient starved
718 *M. smegmatis*. **a**. Proportion of dim cells in MSM-mEos2 cultures grown in nutrient starved
719 conditions with or without the addition of 4mM L-cysteine. Dim cell proportions in each
720 condition were calculated with respect to MSM-mEos2 cultures grown in naïve conditions. Error
721 bars were calculated by measuring standard deviation in dim cell proportions between 10
722 PerSort replicates. **b,c** Time-kill curves of MSM cultures grown in nutrient starved conditions
723 with 4mM L-cysteine and treated with 5x MIC INH (**b**) or 5x MIC RIF (**c**). Time-kill curve data for
724 nutrient rich and nutrient starved conditions (no L-cysteine) is from Figure 1. Data points are
725 averaged from three independent experiments and error bars represent the standard deviation
726 in percent survival between the replicates.
727
728 **Figure 6**. The persister subpopulation converges on a low O_2 metabolic state, which was
729 exploited by addition of L-cysteine to convert the subpopulation to drug susceptible cells. The
730 diagram depicts the processes driving dim (multidrug tolerant persisters) and lit (drug
731 susceptible) cell formation, as discovered through single-cell expression analysis. Evidence from
732 literature further connects these various mechanisms to the O_2 respiratory state of either dim
733 or lit cells. Red arrows indicate connections identified in this study, black arrows are previously
734 determined connections from literature (references indicated), and white boxes are proposed
735 mechanisms for persister cell formation.
736

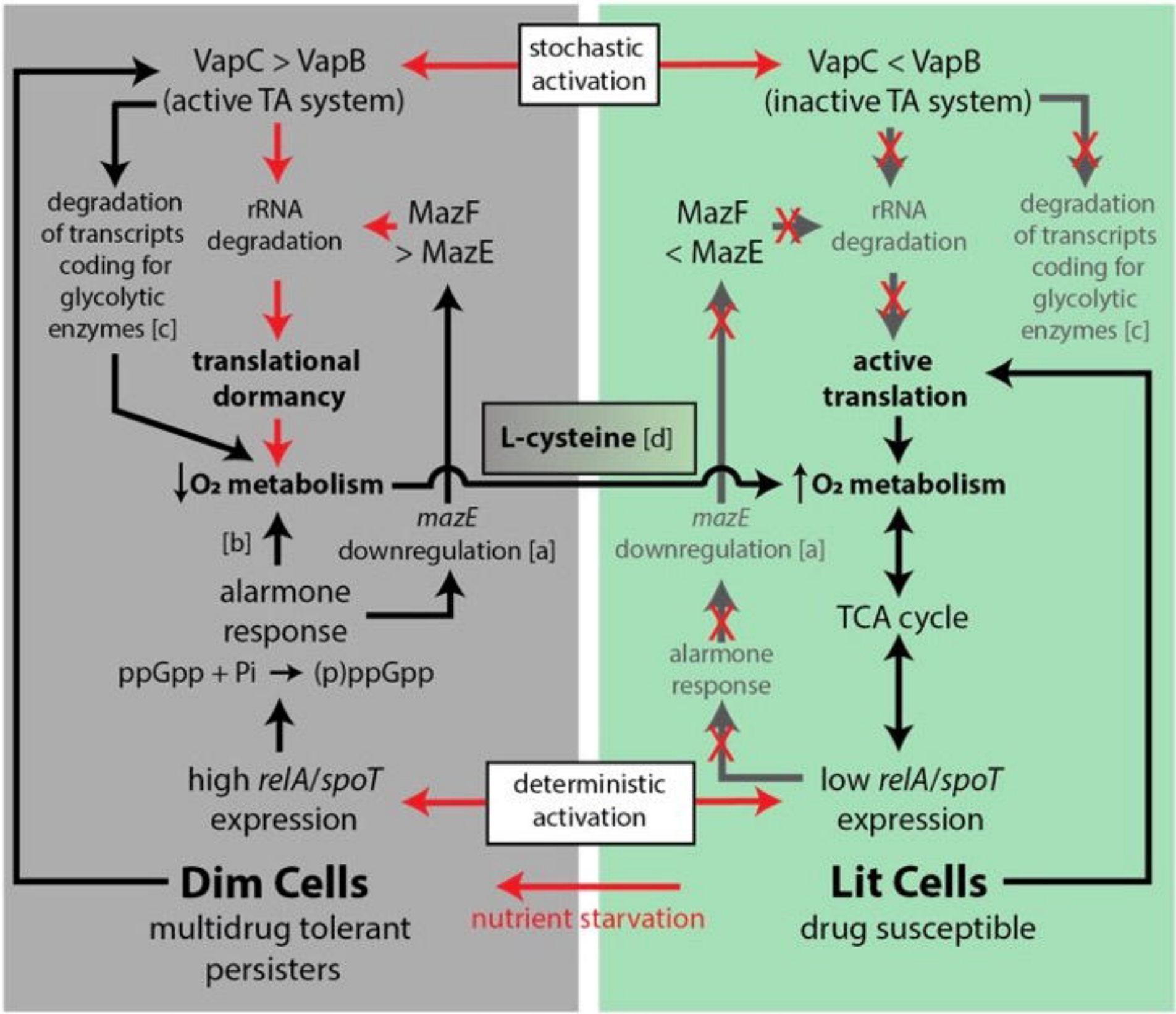

a: Aizenman et al ; b: Verstraeten et al.; c: McKenzie et al.; d: Vilchèze et al.;

Active (this study); Active (literature); Inactive (this study)

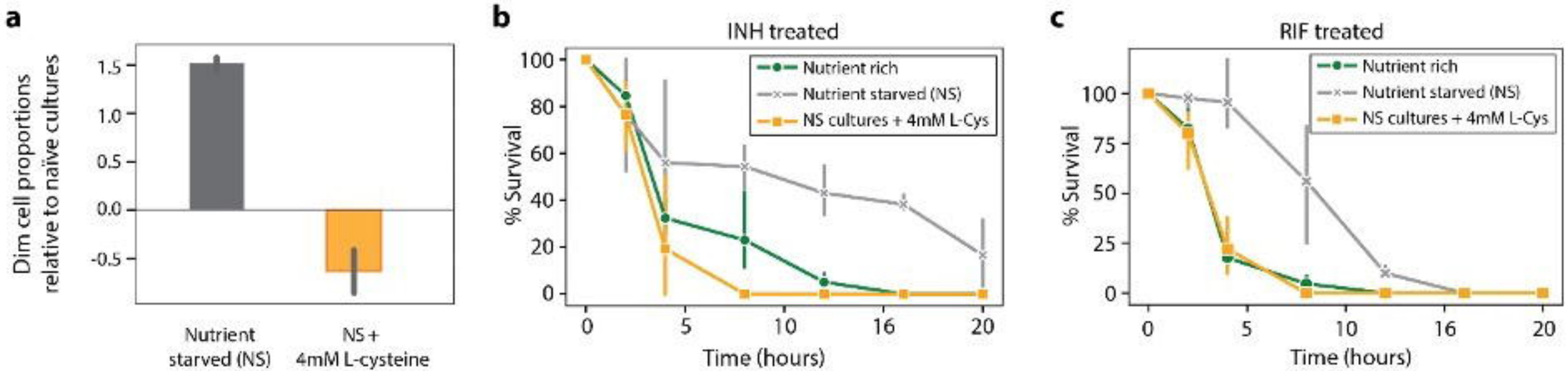
a
Dim cell proportions relative to naïve cultures
1.5
1.0
0.5
0.0
-0.5
Nutrient starved (NS)
NS + 4mM L-cysteine
b
INH treated
% Survival
100
80
60
40
20
0
Nutrient rich
Nutrient starved (NS)
NS cultures + 4mM L-Cys
0
5
10
16
20
Time (hours)
c
RIF treated
% Survival
100
75
50
25
0
Nutrient rich
Nutrient starved (NS)
NS cultures + 4mM L-Cys
0
5
10
16
20
Time (hours)

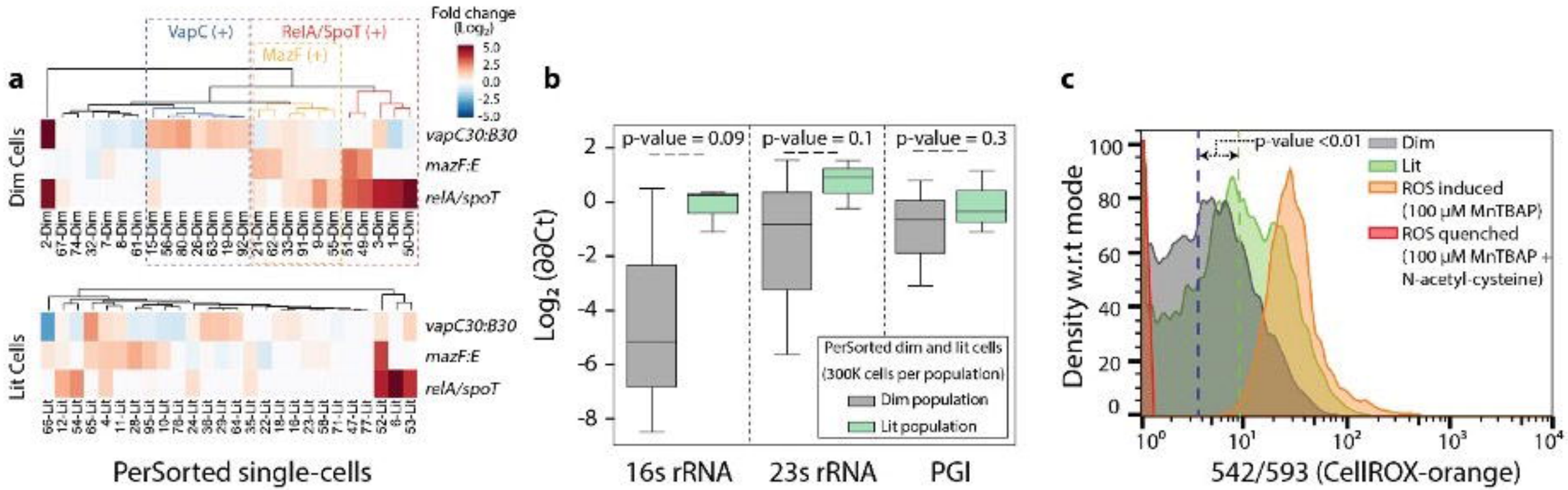
a
VapC (+)
RelA/SpoT (+)
MazF (+)
Fold change (Log2)
5.0
2.5
0.0
-2.5
-5.0
Dim Cells
vapC30:B30
mazF:E
relA/spoT
Lit Cells
PerSorted single-cells
b
p-value = 0.09
p-value = 0.1
p-value = 0.3
Log2 (ΔΔCt)
PerSorted dim and lit cells (300K cells per population)
Dim population
Lit population
16s rRNA
23s rRNA
PGI
c
p-value <0.01
Dim
Lit
ROS induced (100 µM MnTBAP)
ROS quenched (100 µM MnTBAP + N-acetyl-cysteine)
Density w.r.t mode
542/593 (CellROX-orange)

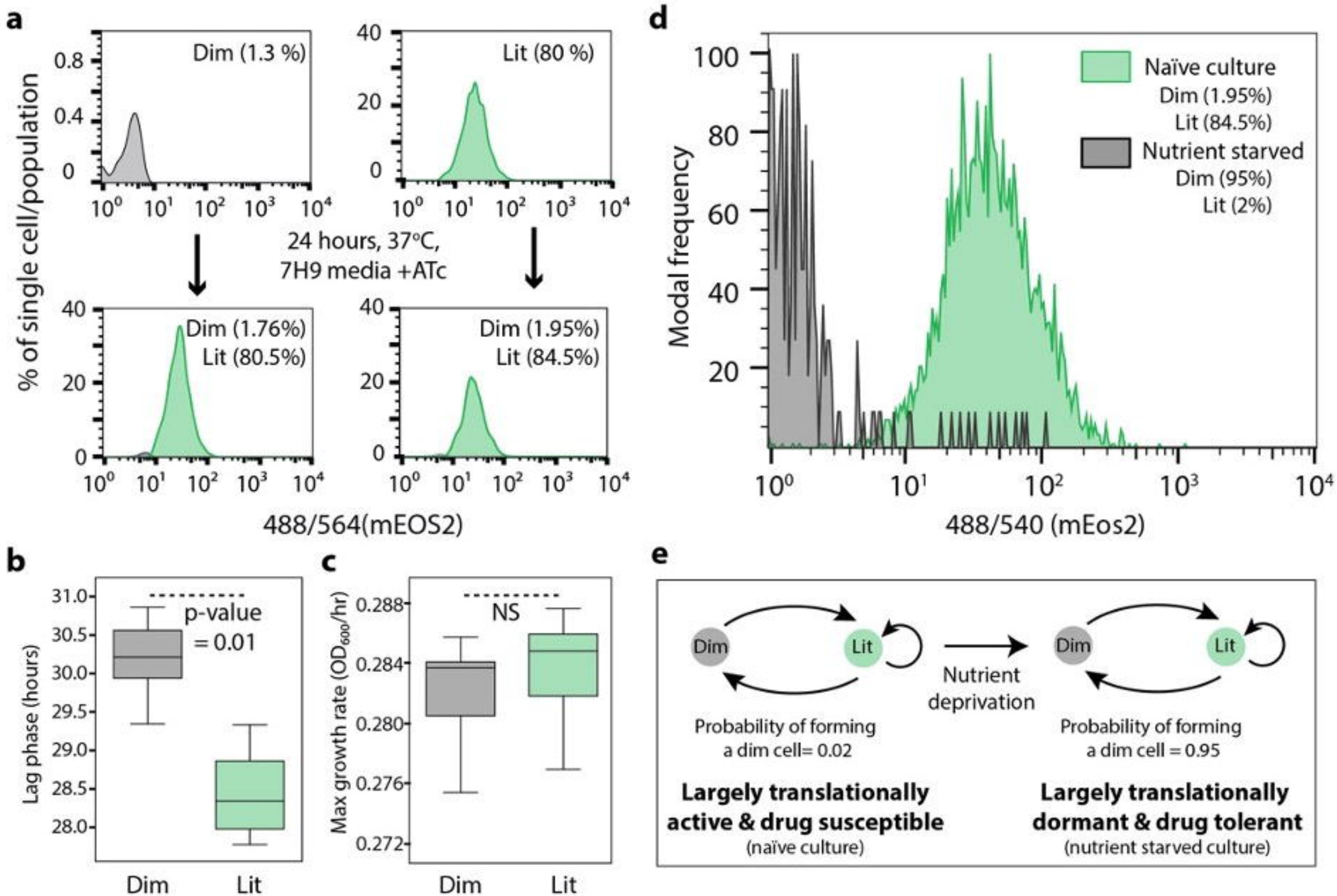
a
Dim (1.3 %)
Lit (80 %)
% of single cell/population
24 hours, 37°C,
7H9 media +ATc
Dim (1.76%)
Lit (80.5%)
Dim (1.95%)
Lit (84.5%)
488/564(mEOS2)
d
Naïve culture
Dim (1.95%)
Lit (84.5%)
Nutrient starved
Dim (95%)
Lit (2%)
Modal frequency
488/540 (mEos2)
b
p-value
= 0.01
Lag phase (hours)
Dim
Lit
c
NS
Max growth rate (OD600/hr)
Dim
Lit
e
Dim
Lit
Nutrient
deprivation
Dim
Lit
Probability of forming
a dim cell= 0.02
Probability of forming
a dim cell = 0.95
Largely translationally
active & drug susceptible
(naïve culture)
Largely translationally
dormant & drug tolerant
(nutrient starved culture)

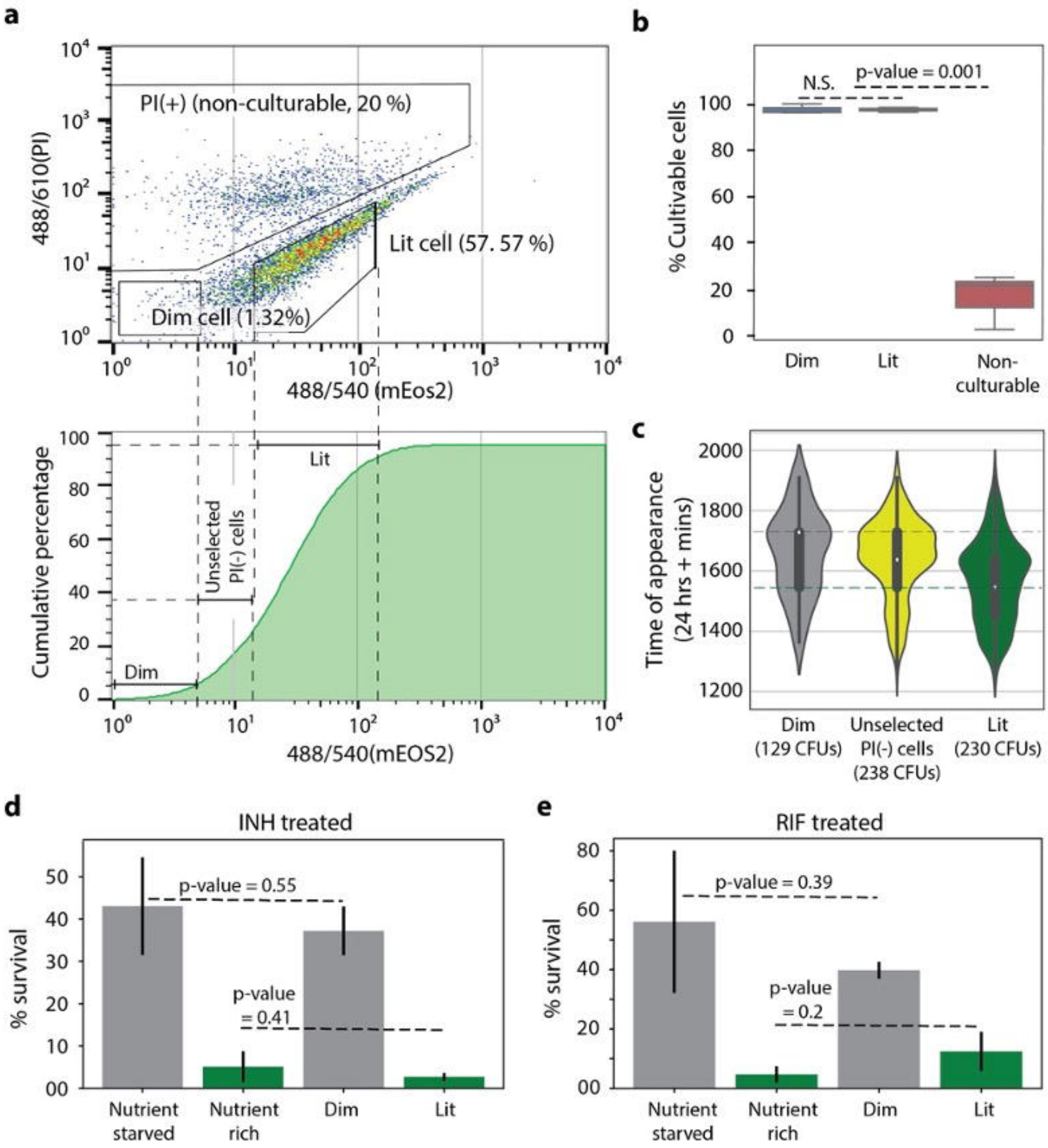
a
PI(+) (non-culturable, 20 %)
Lit cell (57. 57 %)
Dim cell (1.32%)
488/610(PI)
488/540 (mEos2)
Cumulative percentage
Lit
Unselected PI(-) cells
Dim
488/540(mEOS2)
b
N.S.
p-value = 0.001
% Cultivable cells
Dim
Lit
Non-culturable
c
Time of appearance (24 hrs + mins)
Dim (129 CFUs)
Unselected PI(-) cells (238 CFUs)
Lit (230 CFUs)
d
INH treated
p-value = 0.55
p-value = 0.41
% survival
Nutrient starved
Nutrient rich
Dim
Lit
e
RIF treated
p-value = 0.39
p-value = 0.2
% survival
Nutrient starved
Nutrient rich
Dim
Lit

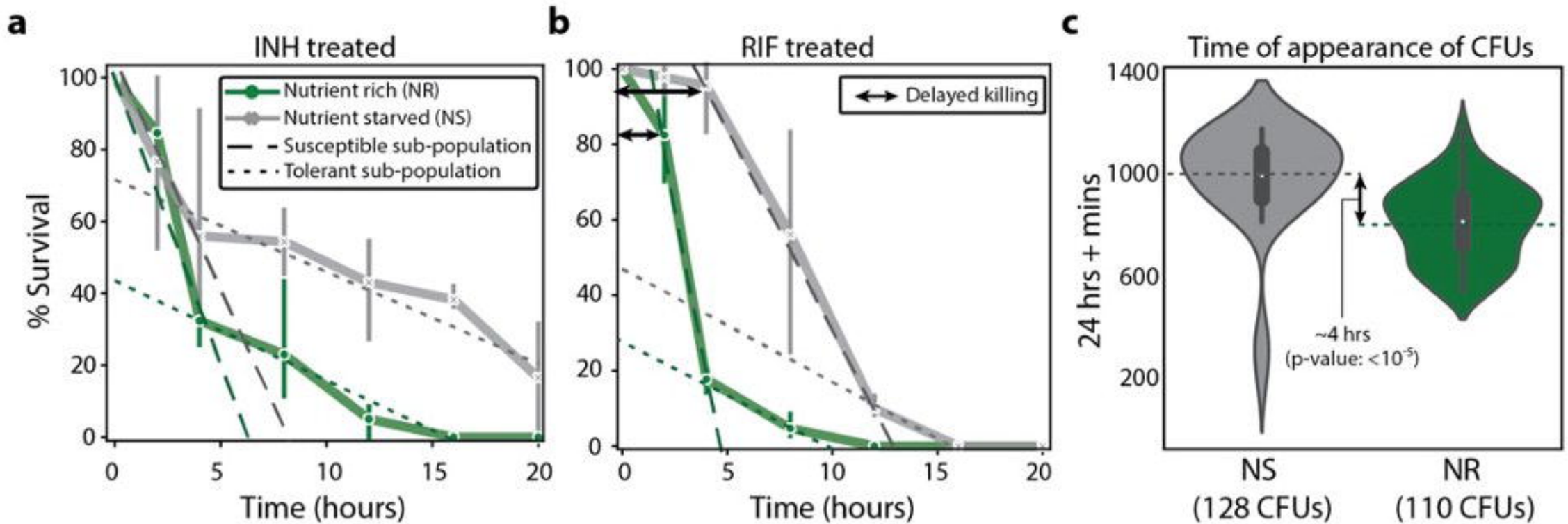
a
INH treated
Nutrient rich (NR)
Nutrient starved (NS)
Susceptible sub-population
Tolerant sub-population
% Survival
Time (hours)
b
RIF treated
Delayed killing
Time (hours)
c
Time of appearance of CFUs
24 hrs + mins
~4 hrs
(p-value: <10^-5)
NS
(128 CFUs)
NR
(110 CFUs)